


Experimental Observation of Magnetic Island Heteroclinic Bifurcation in Tokamaks

L. Bardóczy^{*} and T. E. Evans[✉]

General Atomics, P.O. Box 85608, San Diego, California 92186-5608, USA

 (Received 6 July 2020; revised 26 October 2020; accepted 12 January 2021; published 26 February 2021)

We report empirical observations of magnetic island heteroclinic bifurcation for the first time. This behavior is observed in interacting coupled 2/1 tearing modes in the core of a DIII-D tokamak plasma. Poincaré maps constrained by measured magnetic amplitudes and phasing show bifurcation from heteroclinic to homoclinic topology in the 2/1 island as the 4/2 relative amplitude ($R_{4/2}$) decreases. Initially, the local electron temperature peak in the 2/1 island splits, consistent with two O points. As $R_{4/2}$ decreases a single peak forms, consistent with one O point. These call for developing tearing stability theory and control solutions for heteroclinic islands in tokamaks.

DOI: 10.1103/PhysRevLett.126.085003

Introduction.—Heteroclinic structures are known to be important in atomic and molecular physics [1], solid-state physics [2], laser science [3], nonlinear dynamics [4,5], and in interdisciplinary physics [6]. Recent theory predicts heteroclinic bifurcation of magnetic islands in toroidal plasmas [7,8], which has never been observed in experiments before. This new class of bifurcations is predicted to occur in tokamaks when multiple, rotationally coupled tearing modes (TMs) of the same helicity grow at the same rational surface. For example, an $m/n = 2/1$ island can bifurcate due to an apparent $m/n = 4/2$ TM (m/n are the poloidal/toroidal mode numbers). In this process a second 2/1 island forms within the original 2/1 island, whose O line is not connected to the O line of the original 2/1 island. Hence the resulting composite structure of two 2/1 islands is heteroclinic. Higher order heteroclinic bifurcations can occur if additional $m/n = q$ TMs grow (q is the safety factor, the number of toroidal transits per single poloidal transit of a field line on a toroidal flux surface). This is important, as maintaining good magnetic confinement in tokamaks and preventing instabilities that cause violent disruptive discharge terminations requires active control of 2/1 magnetic islands. Although electron cyclotron current drive (ECCD) is an effective control method of homoclinic islands [9], heteroclinic bifurcation of rotating islands splits the ECCD between the O points, thereby complicating or even preventing stabilization of rotating islands. On the other hand, driving current in multiple O points of locked heteroclinic islands imposes challenges on the EC wave energy and launch geometry. ITER is designed with ECCD capability for homoclinic tearing mode control, but the research plan [10] does not account for the control of heteroclinic islands. Therefore, the experimental study of this new class of bifurcations is crucial for the fundamental understanding of tearing stability and for developing control solutions for heteroclinic islands in tokamaks.

Observations of topological bifurcations within the island interior are enabled by precise local measurements of the electron temperature perturbation (ΔT_e) at the O point. ΔT_e is driven by local static ECCD and is directly manipulated by the magnetic field structure of the islands. Small ΔT_e is quantitatively modeled from first principles by the linear steady state diffusion equation [11,12], which predicts $\Delta T_e \propto \bar{P}_o W^2 / (n_e \chi_\perp)$ in islands characterized by nested flux surface topology. W is the island width, \bar{P}_o is the deposited power density, n_e is the electron density, and χ_\perp is the cross-field electron thermal diffusivity. In a heteroclinic island with two confined regions, one at each of the O points, T_e peaking is expected at each O point. Therefore, a transition from single ΔT_e peak centered at the middle of the island to a split peak with each peak shifted helically can be caused by heteroclinic bifurcation resulting from the formation of two disconnected O points with 2/1 helicity within the original 2/1 island.

Outline.—We report empirical observation of heteroclinic bifurcation in a magnetic island for the first time. In this experiment multiple 2/1 islands grow naturally at $q = 2$. Initially, the 4/2 magnetic amplitude ($A_{4/2}$) is equal to the 2/1 magnetic amplitude ($A_{2/1}$) and a 2/1 island forms with two heteroclinic O points. These are seen from the split of local ΔT_e in the island, where the ΔT_e maxima, each corresponding to one of the two O points, are shifted from the island center by about $\xi \approx \pm\pi/2$. Here $\xi = m\theta - n\phi$ is the helical angle, where θ and ϕ are the poloidal and toroidal angles. Additionally, a higher order heteroclinic bifurcation is triggered, resulting in a third heteroclinic O line in the island interior. Simulations of vacuum islands with zero free parameters show 2/1 islands with heteroclinic O points near $\xi \approx 0, \pm\pi/2$, in accord with the T_e data. $A_{2/1}$ grows faster than $A_{4/2}$, resulting in a natural scan of the 4/2 relative amplitude ($R_{4/2} = A_{4/2}/A_{2/1}$). When $R_{4/2} < 80\%$, the heteroclinic 2/1 island bifurcates to a

homoclinic 2/1 island as seen from the disappearance of the split ΔT_e in accord with simulations showing magnetic topology with a single O point.

Experimental setup.—DIII-D H-mode discharges were studied where the TM naturally forms 2/1 magnetic islands at $\rho \approx 0.52$ (ρ is the square root of the normalized toroidal flux surface label). Relevant plasma parameters include 1.77 m major radius, 0.60 m minor radius, 1.2 MA (I_p) plasma current, 1.9 T toroidal magnetic field in the opposite direction as I_p , zero average loop voltage, 6 MW neutral beam power, constant 2.25 MW electron cyclotron heating (ECH), and 26.5 kA ECCD during the TM evolution. n_e at $q = 2$ is $4.2 \times 10^{19} \text{ m}^{-3}$ [Thomson scattering (TS) [13]] and T_e is 2.4 keV [electron cyclotron emission (ECE) [14] and TS]. The cross-power of magnetic signals shows multiple coherent modes in this plasma [Figs. 1(a) and 1(b)]. Poloidal and toroidal Mirnov-coil array data show that the first three lower frequency modes are characterized by $m/n = 2/1$, $m/n = 4/2$, and $m/n = 6/3$ mode numbers [15,16]. The corresponding frequencies are $f_{2/1} \approx 10$ kHz, $f_{4/2} \approx 20$ kHz, and $f_{6/3} \approx 30$ kHz, respectively. The fourth mode at ≈ 40 kHz is characterized by $n = 4$, but m of this mode cannot be constrained due to the limited number of magnetic probes in the poloidal array. In this Letter we omit the fourth mode due to its very small amplitude. These modes are rotationally coupled to each other throughout the entire analysis window, as seen from the fact that $f_{m/n}/n$ is the same for each mode [Fig. 1(c)]. There are no other strong magnetohydrodynamic (MHD) modes in this plasma. Local ECE T_e data show magnetic islands at $q = 2$ whose frequency and amplitude evolution is consistent with the 2/1 magnetic fluctuations. As the islands rotate by the view of the radially spaced ECE channels the different phases of the islands come into view at different times, enabling us to monitor the internal structure of the entire island. The maximum width of the island is $W_{\text{max}} = 10$ cm when the 2/1 component is 5 times larger than the first subdominant mode. Therefore, these modes are $m/n = 2/1$, $m/n = 4/2$, and $m/n = 6/3$ TMs. The average relative amplitude, $R_{m/n} = A_{m/n}/A_{2/1}$, of the 4/2 (6/3) mode is about $R_{4/2} \approx 100\%$ ($R_{6/3} \approx 80\%$) early in the TM evolution (until about 2800 ms). These are calculated by mapping the probe data at the tokamak wall to the $q = 2$ rational surface location (r_s) using a first principle model in cylindrical geometry as $A_{m/n}(r_s) = A_{m/n}(a)(r_s/a)^{m+1}$ [17,18]. Note that $R_{m/n}(r_s)$ is well constrained in the outboard midplane as it is measured for a relatively long time with 8 toroidally separated probes. Systematic uncertainties arise as this model does not take into account toroidicity and plasma shaping which can impact $A_{m/n}(r_s)$. However, constant geometric factors cancel in the relative amplitudes; therefore we use $R_{m/n}(r_s)$. Fast timescale variations in $A_{2/1}$, $A_{4/2}$, and $A_{6/3}$ emerge due to edge localized modes (ELMs) [Fig. 1(d)], which leads to the variation of $R_{4/2}(r_s)$ [$R_{6/3}(r_s)$] by about 5% [15%]

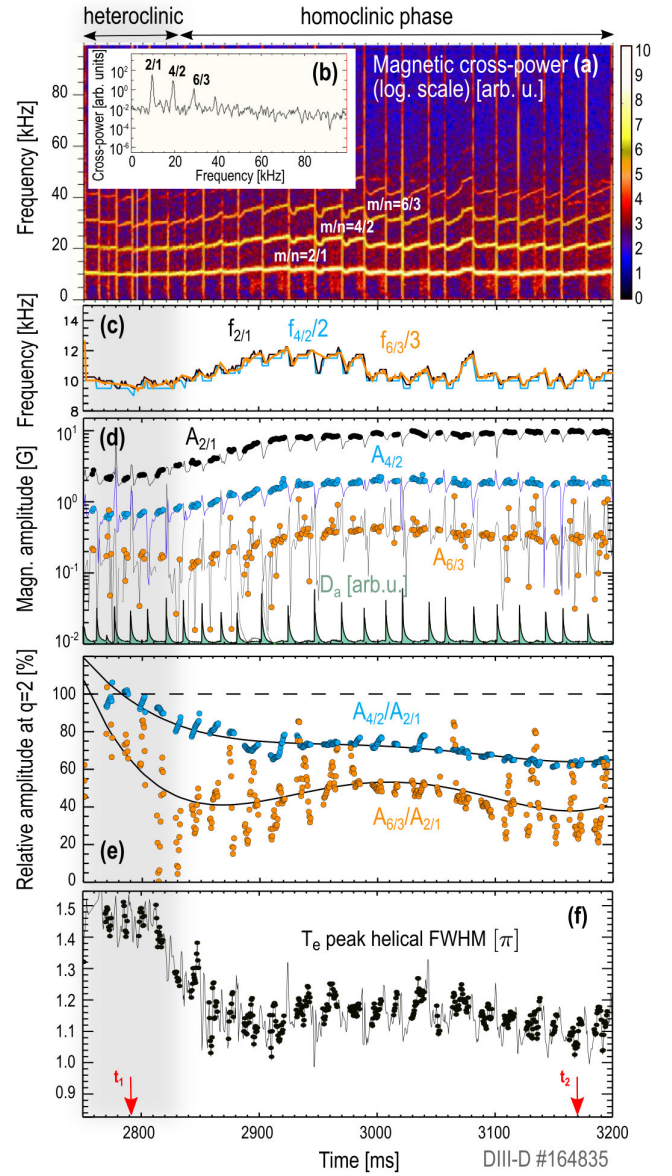


FIG. 1. Cross-power (a) spectrogram and (b) spectrum ($t = 2795$ ms) of magnetic probes. 2/1, 4/2, and 6/3 (c) normalized frequencies and (d) magnetic amplitudes at the wall and D_α signal. (e) $R_{4/2}$ and $R_{6/3}$ at $q = 2$ (lines are third order polynomial fits). (f) Helical FWHM of ΔT_e .

between ELMs. We only use ELM free data points shown with circles in Figs. 1(d)–1(f). Because of the fastest growth of $A_{2/1}$, the relative amplitude $R_{4/2}$ ($R_{6/3}$) decreases to 60% (40%) by 3150 ms. This provides a natural scan of $R_{4/2}$ ($R_{6/3}$) without need to alter plasma conditions externally.

Derivation of ΔT_e at the O point.—ECCD is used to heat the island interior, thereby enabling us to monitor the local magnetic field topology through measurements of the T_e spatial distribution. T_e is obtained via the ECE radiometer that provides measurements of optically thick, second harmonic (X mode) electron cyclotron emission. T_e is probed at 40 radial locations with 500 kHz sampling rate

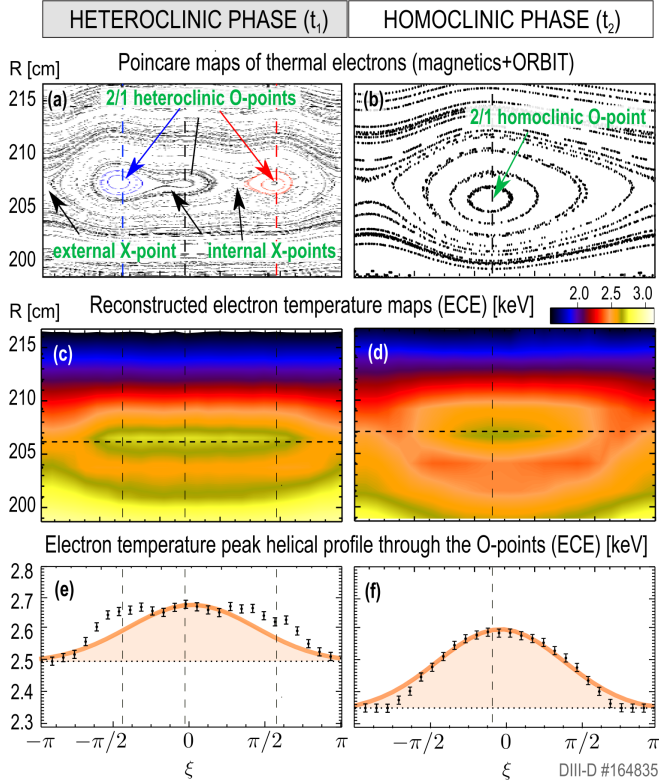


FIG. 2. Poincaré maps in the (a) heteroclinic and (b) homoclinic phase. (c),(d) $T_e(R, \xi)$ maps at the corresponding times of (a),(b), respectively. (e),(f) Helical profiles of T_e through the O point marked with horizontal dashed lines in (c),(d), respectively. Vertical dashed lines mark the O point locations from (a) and (b).

0.3 cm above the low-field side midplane at $\phi = 81^\circ$ toroidal angle. The island rotation enables the probing of T_e with respect to the helical phase. T_e is transformed from the lab frame to the island frame via phase-lock averaging [$T_e(R, t) \rightarrow T_e(R, \xi)$] as in earlier work, which removes the rotation and greatly reduces the noise [19] [Figs. 2(c) and 2(d)]. The mapping $t \rightarrow \xi$ is based on the identification of the X point passing by times of the main island, which are given by the minima of $T_e(r > r_s, t)$. This holds regardless of the details of the internal structure of this island, i.e., if homoclinic or bifurcated to multiple heteroclinic structures. Helical $T_e(R_o, \xi)$ profiles that go through the O point are shown in Figs. 2(e) and 2(f). We estimate the radial coordinate (R_o) of the O point(s) as the extremum location of a second order polynomial fit on the maximum of $T_e(R, \xi_o)$ and one neighboring point on each side. $T_e(R_o, \xi)$ is then obtained by interpolating $T_e(R, \xi)$ at R_o . Note that there are typically about 50 independent $T_e(R_o, \xi)$ measurements in each island cycle as T_e is sampled with 500 kHz and the island rotates with about 10 kHz. ΔT_e is wide (FWHM $\approx 1.45\pi$) initially when $R_{4/2} \approx 100\%$, and this width is nearly constant until $R_{4/2}$ drops to about 85% [Fig. 1(f)]. As $R_{4/2}$ further decreases, ΔT_e rapidly narrows and stays about constant thereafter

(FWHM $\approx 1.15\pi$). This behavior of ΔT_e indicates the existence of 2 preferred states, one at FWHM = 1.45π and one at FWHM = 1.15π . To calculate if heteroclinic bifurcation should be occurring in this equilibrium with the measured magnetic modes, we derive the magnetic field structure of the islands at $q = 2$ by constructing Poincaré maps via the ORBIT code [20].

Structure of vacuum islands.—ORBIT solves the Hamiltonian guiding center equations in the ideal limit, where any parallel electric field perturbations are canceled by the fast response of electrons along the magnetic field. The magnetic field is a superposition of the experimentally reconstructed Grad-Shafranov equilibrium and three non-axisymmetric perturbations represent the 2/1, 4/2, and 6/3 TMs. The equilibrium is found using the code EFIT [21], constrained by internal measurements of the poloidal field radial profile by motional Stark effect spectroscopy [22] and by external magnetic probes [15]. The perturbation of a single TM with m and n mode numbers is $\tilde{\mathbf{B}}_{m,n}(r, \xi(t), t) = \nabla \times (\hat{z}\psi_{m,n}(r, \xi(t), t))$, where $\psi_{m,n}(r, \xi(t), t) = \psi_{m,n}(r, t)\psi_{m,n}(\xi(t))$. Here the large tokamak approximation is used and \hat{z} is the unit vector in the z direction in cylindrical coordinates. The helical part $\psi_{m,n}(\xi(t)) = \cos(m\theta - n\phi + 2\pi f_{m,n}(t)t + \xi_{m,n}^\circ)$ prescribes the three-dimensional structure in Boozer coordinates and the rotation ($\xi_{m,n}^\circ$ are initial phases). The radial structure, $\psi_{m,n}(r, t)$, prescribes the magnetic field of a helical current perturbation as in earlier work [18]. $\psi_{m,n}(r, t)$ decays as r^{-m-1} and produces a finite value at the probe location which is used to match these simulations to the measurements. In the initial phase, $R_{4/2}(r_s, t_1) = 1$ and $R_{6/3}(r_s, t_1) = 0.6$, and in the final phase, $R_{4/2}(r_s, t_3) = 0.6$ and $R_{6/3}(a, t_3) = 0.4$. In each phase, the absolute amplitude of the dominant mode is set by matching the resultant island width to the measured ECE island width. The frequencies are fixed, $f_{2/1} = f_{4/2}/2 = f_{6/3}/3 = f = 10$ kHz, at each time slice. The exact value of f has no significance as long as the islands are coupled. The phases are $\xi_{2/1}^\circ = 0$, $\xi_{4/2}^\circ = \pi/2$, and $\xi_{6/3}^\circ = 0$. The two times t_1 and t_2 are marked in Fig. 1(f).

The Poincaré map of the initial phase (t_1) in Fig. 2(a) shows that two heteroclinic O Points form near $\pm\pi/2$. These are asymmetric in magnitude and the one at $-\pi/2$ stretches toward $\xi = 0$. These two O points are not connected with each other, which is a strong geometric constraint as single closed loops with $m = 4$, $n = 2$ mode numbers do not exist on a torus. This is also seen from simulations where field lines in one O point are confined within that region without traveling to the other O point, shown in Fig. 2(a) by coloring the field lines that belong to each O point. A strong enough 6/3 triggers a higher order heteroclinic bifurcation which forms a third disjoint small O point near $\xi = 0$. The magnetic field structure in this phase is consistent with a heteroclinic 2/1 island.

In the *final* phase (t_2), when the 4/2 and 6/3 amplitudes are sufficiently small, a clear O point forms slightly shifted from the center of the island with no additional internal O points or X points. This structure is consistent with a homoclinic 2/1 island, whose helical asymmetry is caused by the finite $R_{4/2}$ and $R_{6/3}$.

In conclusion, these simulations show that a bifurcation from heteroclinic to homoclinic topology is occurring in this DIII-D discharge. In the following we report evidence in local T_e data supporting this claim.

Evidence of heteroclinic bifurcation in local T_e .—The $T_e(R, \xi)$ heat maps in Figs. 2(c) and 2(d) and the $T_e(R_o, \xi)$ helical profiles in Figs. 2(e) and 2(f) demonstrate characteristic changes consistent with formation or disappearance of multiple internal O points in the T_e distribution within the island as $R_{4/2}$ and $R_{6/3}$ decrease in this plasma. Note that the magnetic fluctuations are higher harmonics of each other; hence stochasticization is not expected. The observed clear peak in the T_e radial profile at r_s confirms that good thermal confinement exists within the islands, consistent with nested flux surface topology. Without attempting to model T_e in the two phases, we overplot a Gaussian in each case for ease of comparison between Figs. 2(e) and 2(f). The parameters of this Gaussian are determined by least square fitting in the homoclinic phase [Fig. 2(f)], where this model is a good fit. In the heteroclinic phase the baseline is $T_e(\xi = 0)$, the amplitude is normalized to match the maximum of T_e near the island center, and the width is kept the same as in the homoclinic phase so that the changes of ΔT_e caused by the bifurcation can be clearly observed.

In the initial phase ΔT_e is wide (FWHM = 1.45π) and, compared to a Gaussian, the T_e distribution shows two lobes near $\pm\pi/2$. The location and width of these peaks are consistent with the heteroclinic O points of the Poincaré map in Fig. 2(a). Interestingly, the T_e peak at $-\pi/2$ is more pronounced than the one at $\pi/2$. This helical asymmetry is also consistent with the Poincaré map in Fig. 2(a). Between the two helically shifted peaks, there is a third peak near $\xi = 0$. This volume is occupied by another O point which gives rise due to the higher order heteroclinic bifurcation consistent with the 6/3 magnetic structure and the Poincaré plot. Therefore, these local T_e data are consistent with a heteroclinic island characterized by three O points residing at $\xi = 0, \pm\pi/2$.

In the final phase the Gaussian is a good fit to the points of ΔT_e , in contrast to the initial phase. ΔT_e is characterized by a single maximum in agreement with observations in homoclinic islands of plasmas with a single TM. These data are also consistent with the Poincaré map in Fig. 2(b).

The ΔT_e helical FWHM correlates with $R_{4/2}$ and the points of the heteroclinic phase clearly isolate from the points of the homoclinic phase in Fig. 3. This supports that the ΔT_e splitting in Fig. 2(c) is caused by the 4/2 TM, in accord with the O -point splitting due to the 4/2 TM in the experimentally constrained Poincaré map in Fig. 2(a).

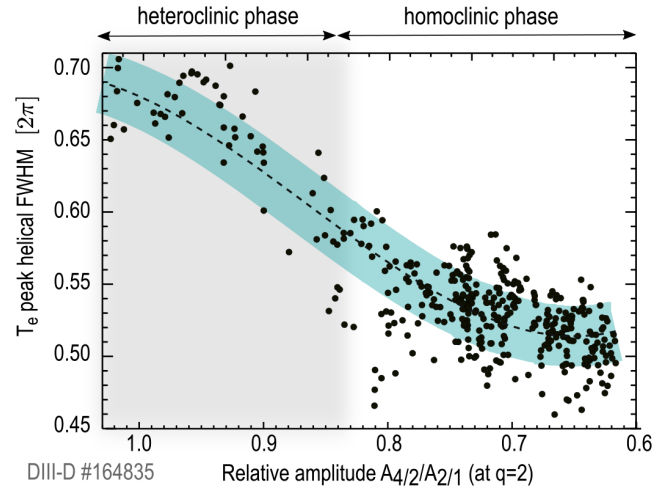


FIG. 3. Helical FWHM of ΔT_e peak with respect to $R_{4/2}$.

As an alternative explanation, large diffusivity within the island could cause flattening, but it falls short in explaining (i) that flattening occurs only in the middle region, (ii) the helically stretched structure, and (iii) the correlation with the 4/2 amplitude. On the other hand, another, toroidally coupled island chain with $m/n \neq 2$ could cause stochasticization which then could modify ΔT_e within the island. There are no islands on other rational surfaces in this plasma, however. Finally, a rapid modulation of the $f_{2/1}$ within the island revolution cycle could result in a false 4/2 component in the measured magnetic signals. This can be addressed by analysis of the mode spatial structure from toroidal array of magnetic probes which confirms that the $n = 2$ component comes from a plasma mode and not from modulation of the 2/1 rotation. We conclude that there is no better explanation of the reported data than the heteroclinic bifurcation [7,8].

Summary.—We have reported empirical observations of heteroclinic bifurcation in magnetic islands for the first time. In this experiment, a 2/1 and a 4/2 TM grow simultaneously and compete to form islands in the same volume of a tokamak plasma core. Poincaré maps are used to characterize the magnetic structure of the islands, where the simulation input parameters are derived from and fully constrained by magnetic probe data. In addition, reconstruction of the local T_e profile within the rotating island is used to characterize the island internal structure. When $R_{4/2} = 100\%$ the simulations show that the 2/1 island is heteroclinic with 3 O points. At this time, ΔT_e is split at $q = 2$, and the split peaks are located at $\xi \approx 0, \pm\pi/2$ in accord with the O points in the Poincaré maps. The faster 2/1 growth then results in a natural scan of $R_{4/2}$ (and $R_{6/3}$). When $R_{4/2}$ ($R_{6/3}$) decreases below 80% (60%), the heteroclinic 2/1 island bifurcates to a homoclinic 2/1 island, as seen from the disappearance of the split ΔT_e . At this time a single ΔT_e is centered at the middle of the island in accord with vacuum island simulations showing a single O point

near the island center. Our measurements therefore give a clear and unambiguous demonstration that heteroclinic bifurcation of magnetic islands can occur in tokamaks. This phenomenon can be crucial for disruption avoidance via ECCD stabilization of the deleterious 2/1 islands, as the EC wave energy splits between the two heteroclinic O points which may make the stabilization of rotating 2/1 islands harder. On the other hand, driving current in both of the heteroclinic O points of locked islands imposes challenges on the EC wave launch geometry which is not accounted for in present tokamaks or in the ITER research plan.

The authors acknowledge very useful discussions with T. E. Strait, N. C. Logan, and M. Podesta. This material is based upon work supported by the U.S. Department of Energy, Office of Science, Office of Fusion Energy Sciences, using the DIII-D National Fusion Facility, a DOE Office of Science user facility, under Awards No. DE-FC02-04ER54698 (L. B. and T. E. E.) and No. DE-SC0018030 (T. E. E.). This Letter was prepared as an account of work sponsored by an agency of the U.S. Government. Neither the U.S. Government nor any agency thereof, nor any of their employees, makes any warranty, express or implied, or assumes any legal liability or responsibility for the accuracy, completeness, or usefulness of any information or represents that its use would not infringe privately owned rights. The views and opinions of authors expressed herein do not necessarily state or reflect those of the U.S. Government or any agency thereof.

*bardoczil@fusion.gat.com

- [1] M. Conforti, A. Mussot, A. Kudlinski, S. Rota Nodari, G. Dujardin, S. D. Bièvre, A. Armaroli, and S. Trillo, *Phys. Rev. Lett.* **117**, 013901 (2016).
- [2] Y. Lei and R. Fu, *Europhys. Lett.* **112**, 60005 (2016).
- [3] M. Finardi, L. Flepp, J. Parisi, R. Holzner, R. Badii, and E. Brun, *Phys. Rev. Lett.* **68**, 2989 (1992).
- [4] E. Stone, M. Gorman, M. el Hamdi, and K. A. Robbins, *Phys. Rev. Lett.* **76**, 2061 (1996).
- [5] M. I. Rabinovich, R. Huerta, and P. Varona, *Phys. Rev. Lett.* **96**, 014101 (2006).
- [6] M. Rabinovich, A. Volkovskii, P. Lecanda, R. Huerta, H. D. I. Abarbanel, and G. Laurent, *Phys. Rev. Lett.* **87**, 068102 (2001).
- [7] T. E. Evans, W. Wu, G. P. Canal, and N. M. Ferraro, [arXiv:1805.10394](https://arxiv.org/abs/1805.10394).
- [8] W. Wu, T. Evans, G. Canal, N. Ferraro, B. Lyons, and D. Orlov, *Nucl. Fusion* **59**, 066010 (2019).
- [9] R. J. L. Haye, S. Gunter, D. A. Humphreys, J. Lohr, T. C. Luce, M. E. Maraschek, C. C. Petty, R. Prater, J. T. Scoville, and E. J. Strait, *Phys. Plasmas* **9**, 2051 (2002).
- [10] I. Organization, ITER research plan within the staged approach (2018), https://www.iter.org/doc/www/content/com/Lists/ITER%20Technical%20Reports/Attachments/9/ITER-Research-Plan_final_ITR_FINAL-Cover_High-Res.pdf.
- [11] R. Fitzpatrick, *Phys. Plasmas* **2**, 825 (1995).
- [12] L. Bardóczi, T. L. Rhodes, T. A. Carter, A. B. N. R. J. La Haye, and G. R. McKee, *Phys. Plasmas* **24**, 062503, 023502 (2017).
- [13] T. N. Carlstrom, G. L. Campbell, J. C. DeBoo, R. Evanko, J. Evans, C. M. Greenfield, J. Haskovec, C. L. Hsieh, E. McKee, R. T. Snider *et al.*, *Rev. Sci. Instrum.* **63**, 4901 (1992).
- [14] M. E. Austin and J. Lohr, *Rev. Sci. Instrum.* **74**, 1457 (2003).
- [15] E. J. Strait, *Rev. Sci. Instrum.* **77**, 023502 (2006).
- [16] J. D. King, E. J. Strait, R. L. Boivin, D. Taussig, M. G. Watkins, J. M. Hanson, N. C. Logan, C. Paz-Soldan, D. C. Pace, D. Shiraki *et al.*, *Rev. Sci. Instrum.* **85**, 083503 (2014).
- [17] J. Wesson, *Tokamaks* (Oxford University Press, New York, 2011).
- [18] L. Bardóczi, M. Podestà, W. W. Heidbrink, and M. A. V. Zeeland, *Plasma Phys. Controlled Fusion* **61**, 055012 (2019).
- [19] L. Bardóczi, T. L. Rhodes, T. A. Carter, N. A. Crocker, W. A. Peebles, and B. A. Grierson, *Phys. Plasmas* **23**, 052507 (2016).
- [20] R. B. White and M. S. Chance, *Phys. Fluids* **27**, 2455 (1984).
- [21] L. Lao, J. Ferron, R. Groebner, W. Howl, H. S. John, E. Strait, and T. Taylor, *Nucl. Fusion* **30**, 1035 (1990).
- [22] D. Wróblewski and L. L. Lao, *Rev. Sci. Instrum.* **63**, 5140 (1992).